Investigation of side wall and ship model interaction

Zhi-Ming Yuan*, Atilla Incecik

Department of Naval Architecture, Ocean and Marine Engineering
University of Strathclyde, Glasgow, G4 0LZ, UK

Abstract: Due to the existence of the side wall of the towing tank, the measured hydrodynamic forces would present some discrepancies compared to the open sea results. This phenomenon is referred as side wall effect. The object of the present study is to investigate the parameters which determine the side wall effects. The method used in the present study involves a 3D panel method based on Rankine type Green function. A ship advancing in a towing tank with parallel side walls is simulated and the numerical results are validated against model test results carried out by Kashiwagi and Ohkusu (1991). The parameters including wave frequency and forward speed which determine the side wall effects are discussed.
Keywords: Side wall effects; Rankine source method; Hydrodynamic interaction; Wave pattern; Forward speed.
Article ID: H104

1 Introduction

A ship model towing tank always has a limited breadth. Due to the existence of the side walls of the towing tank, the measured hydrodynamic forces would present some discrepancies compared to the open water results. This phenomenon is referred as side wall effect. There are many factors which determine the side wall effects. These factors include the ship geometry, breadth of the tank and forward speed of the ship model. In seakeeping tests, the oscillating frequency is another critical parameter which must be taken into consideration. For a certain combination of the above parameters, the measurements from the tests could differ significantly from the open sea results. The object of the present work is to find the relation between the side wall effects and the parameters which determine the side wall effects. Based on the purpose of the ship model test in a towing tank, the side wall may affect the measurements in wave-making problem and seakeeping problem.

The side wall effects on model test in calm water is not very obvious and therefore it is usually neglected in the model tests. In calm water, the side wall effects can be simply estimated by Kelvin wave pattern, as shown in Fig. 1. The waves produced at the bow are reflected by the vertical side walls, and these reflected waves will strike the ship if the distance d is very small. The minimum distance d_m can be estimated as

$$d_m = \frac{1}{2} L \tan\theta \approx 0.18L \tag{1}$$

It indicates if the distance between the ship and side wall is larger than $0.18L$, the side wall effects can be neglected in ship model test in calm water. It should be pointed out that this minimum distance d_m will be modified by the near field local waves produced by a 3D ship. Therefore, d_m is slightly larger than the estimated value from Eq. (1). However, it will not overturn the conclusion that d_m is much smaller than ship length L. In practice, the breadth of most of the towing tanks is larger than $2d_m$. Therefore, the side wall effects are neglected in wave-making problem, and the studies on side wall effects on calm water model test are very rare. But a ship advancing in a channel is widely studies (Beck et al., 1975; Mei and Choi, 1987; Norrbin, 1974; Tuck, 1978). Theoretically, these two topics are very similar. The difference is that in a towing tank, the ship model is usually fixed in the center line of the tank (as shown in Fig. 1). There is no force (or moment) components in y direction. But for a ship maneuvering in a canal or channel, it is very difficult to guarantee the ship is always advancing along the center line of the canal. Therefore, there is a lateral force, as well as a yaw moment acting on the ship.

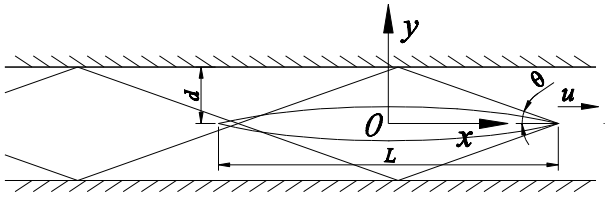

Fig. 1 A sample ship advancing in a towing tank, where d is the distance between the ship and side wall and θ is the semi-wedge angle of the waves produced by the ship. In calm water, the semi-wedge angle $\theta = \sin^{-1}(1/3) \approx 19.47°$.

The side wall effects on ship model test in waves are more complicate than that in calm water due to the factor of oscillating frequency. In order to investigate the side wall effects on ship model test in waves, another critical parameter τ ($\tau = \omega_e u/g$, ω_e is the encounter frequency, u is the forward speed, and g is the gravity acceleration) should be introduced. Due to the oscillating and translating properties, there are three individual wave systems as the parameter $\tau < 0.25$

Received date: 25/03/2016
Foundation item: Funded by the European commission under contract No. 605221.
***Corresponding author Email: zhiming.yuan@strath.ac.uk**

(Becker, 1958; Noblesse and Hendrix, 1992; Yuan et al., 2015b). Correspondingly, the semi-wedge angles are not constant anymore. They are determined by parameter τ. Besides, the semi-wedges angle of the waves produced by an oscillating source are larger than Kelvin wedge. Therefore, the side wall effects have to be taken into consideration during the model test in towing tank. Kashiwagi and Ohkusu (1989, 1991) used the asymptotic wave contour to estimate the side-wall effect. They also extended Newman's (Newman, 1978) unified slender-ship theory and developed a new method to calculate the side-wall effects numerically. The critical line obtained numerically was presented and compared to the results estimated from asymptotic wave contour. A diagram which shows whether side wall effects are expected was presented in Kashiwagi's study (Kashiwagi and Ohkusu, 1991). Similar studies are also carried out by Hosoda (1976; 1979). These studies are based on slender ship theory. Iwashita (2001) used a 3D Rankine panel method to investigate the unsteady waves in low frequency range. There are many advantages of using Rankine source panel method. But a radiation condition on control surface is required, especially when the parameter $\tau < 0.25$.

In this paper, a so-called Sommerfeld radiation condition with forward speed correction is imposed on the control surface to ensure that the waves can propagate to the far field without reflection. This radiation condition is included in our in-house developed program MHydro, which is well validated with experiments (Yuan et al., 2015a; Yuan et al., 2014a; Yuan et al., 2014b; Yuan et al., 2015d).

2 2 Mathematical formulation

2.1 Boundary value problem of steady flow

When a ship advances at constant speed in calm water, it will generate steady waves and induce the so-called wave-making resistance. It is assumed that the fluid is incompressible and inviscid and the flow is irrotational. The velocity potential can be expressed as

$$\varphi_{Ts} = ux + \varphi_s \tag{2}$$

φ_s satisfies the Laplace equation

$$\nabla^2\varphi_s = 0 \quad \text{in the fluid domain} \tag{3}$$

Following Newman (1976), the nonlinear dynamic free-surface condition on the disturbed free surface can be expressed as

$$u\frac{\partial\varphi_s}{\partial x} + \frac{1}{2}\left[\left(\frac{\partial\varphi_s}{\partial x}\right)^2 + \left(\frac{\partial\varphi_s}{\partial y}\right)^2 + \left(\frac{\partial\varphi_s}{\partial z}\right)^2\right] + g\zeta = 0, \quad \text{on } z = \zeta(x,y) \tag{4}$$

The kinematic free-surface condition is

$$u\frac{\partial\zeta}{\partial x} - \frac{\partial\varphi_s}{\partial z} + \frac{\partial\varphi_s}{\partial y}\frac{\partial\zeta}{\partial y} + \frac{\partial\varphi_s}{\partial x}\frac{\partial\zeta}{\partial x} = 0, \quad \text{on } z = \zeta(x,y) \tag{5}$$

The first approximation is based on the linear free surface conditions on the undisturbed water surface. By neglecting the nonlinear terms in Eq. (4) and (5), we can obtain the linear classic free surface boundary condition

$$u^2\frac{\partial^2\varphi_s}{\partial x^2} + g\frac{\partial\varphi_s}{\partial z} = 0, \text{ on the undisturbed free surface} \tag{6}$$

For the ship-to-ship with same forward speed problem, the body surface boundary condition can be written as

$$\frac{\partial\varphi_s}{\partial n} = u\cdot n_1, \quad \text{on the mean wetted body surface} \tag{7}$$

where $\vec{\mathbf{n}} = (n_1, n_2, n_3)$ is the unit normal vector inward on the wetted body surface of the ship. The boundary condition on the sea bottom and side walls can be expressed as

$$\frac{\partial\varphi_s}{\partial n} = 0, \quad \text{on } z = -h \text{ and side walls} \tag{8}$$

The radiation condition is satisfied by using second-order upwind differential scheme.

2.2 Boundary value problem of unsteady flow

It is assumed that the surrounding fluid is inviscid and incompressible, and that the motion is irrotational, the total velocity potential exists which satisfies the Laplace equation in the whole fluid domain. Let t denote time and $\vec{\mathbf{x}} = (x, y, z)$ the position vector. A complex velocity potential provides a description of the unsteady flow as

$$\psi(\vec{\mathbf{x}}, t) = \mathrm{Re}\sum_{j=0}^{7}\eta_j\varphi_j(x, y.z)e^{-i\omega_e t} \tag{9}$$

where φ_j (j = 1,2,…,6) are the spatial radiation potential in six degrees of freedom corresponding to the oscillations of the ship and η_j *(j=1,2,…6)* is the corresponding motion amplitude (η_1, surge; η_2, sway; η_3, heave; η_4, roll; η_5, pitch; η_6, yaw); $\eta_7=\eta_0$ is the incident wave amplitude; φ_7 is the spatial diffraction potential; φ_0 is the spatial incident wave potential and ω_e is the encounter frequency, which can be written as

$$\omega_e = \omega - uk\cos\beta \tag{10}$$

Linear wave theory provides the potential for unit-amplitude incident waves as

$$\varphi_0 = -\frac{ig}{\omega}\frac{\cosh k(z+h)}{\cosh kh}e^{i[k(x\cos\beta + y\sin\beta)]} \tag{11}$$

where $k = \omega^2/g$ is the wave number, ω is the incident wave frequency, h is the water depth, β is the angle of wave heading (β =180 deg. corresponds to head sea).

The unsteady perturbation potential φ_j can be solved by the following boundary value problem:

$$\nabla^2\varphi_j = 0 \quad \text{in the fluid domain} \tag{12}$$

$$-\omega_e^2\varphi_j - 2i\omega_e u\frac{\partial\varphi_j}{\partial x} + u^2\frac{\partial^2\varphi_j}{\partial x^2} + g\frac{\partial\varphi_j}{\partial z} = 0 \quad \text{on the undisturbed free surface } S_f \tag{13}$$

$$\frac{\partial\varphi_j}{\partial z} = 0 \quad \text{on the sea bottom} \tag{14}$$

$$\frac{\partial\varphi_j}{\partial n} = \begin{cases} -i\omega_e n_j + m_j, \; j = 1,2,...,6 \\ -\dfrac{\partial\varphi_0}{\partial n}, \; j = 7 \end{cases} \quad \text{on the mean wetted part of the body surface } S_b \tag{15}$$

The radiation condition at infinity is also imposed to

complete the boundary value problem. The generalized normal vectors are defined as

$$n_j = \begin{cases} \vec{n},\ j = 1,2,3 \\ \vec{x} \times \vec{n},\ j = 4,5,6 \end{cases} \tag{16}$$

and $\vec{n} = (n_1, n_2, n_3)$ is the unit normal vector directed inward on body surface S_b, $\vec{x} = (x, y, z)$ is the position vector on S_b. The m_j denotes the j-th component of the so-called *m*-term, which can be expressed as

$$m_j = \begin{cases} -(\vec{n} \cdot \nabla)\nabla\varphi_s,\ j = 1,2,3 \\ -(\vec{n} \cdot \nabla)(\vec{x} \times \nabla\varphi_s),\ j = 4,5,6 \end{cases} \tag{17}$$

The m-terms provide coupling effects between the steady and unsteady flows and involve the second derivatives of the steady potential. However, in the present study, we are interested in the very low forward speed problem. Therefore, the Neumann-Kelvin linearization can be used to simplify the *m*-terms,

$$\begin{aligned} (m_1, m_2, m_3) &= (0,0,0) \\ (m_4, m_5, m_6) &= (0, n_3, -n_2) \end{aligned} \tag{18}$$

Besides, a Sommerfeld radiation condition with forward speed correction is imposed on the control surface to ensure that the waves can propagate to the far field without reflection.

2.3 Wave-making resistance and hydrodynamic forces

Once the unknown potential φ_s and φ_j are solved, the steady pressure and the time-harmonic pressure can be obtained from Bernoulli's equation:

$$p_s = \rho\left(u\frac{\partial\varphi_s}{\partial x} - \frac{1}{2}\nabla\varphi_s \cdot \nabla\varphi_s \right) \tag{19}$$

$$p_j = -\rho\left[i\omega_e\varphi_j + \nabla(\varphi_s - ux) \cdot \nabla\varphi_j \right],\ j = 0,\ 1,\ldots,\ 7 \tag{20}$$

The steady hydrodynamic forces are obtained by the pressure integral on the wetted body surface as follows:

$$F_i^s = \iint_{S_b} p_s n_i dS,\ \ i = 1,\ 2,\ \ldots,\ 6 \tag{21}$$

The wave making resistance can be defined as

$$C_w = \frac{F_1^s}{\frac{1}{2}\rho u^2 S} \tag{22}$$

where S is the area of the wetted body surface. The hydrodynamic force produced by the oscillatory motions of the vessel in the six degrees of freedom can be derived from the radiation potential as

$$F_i^R = \sum_{j=1}^{6} \iint_{S_b} p_j n_i dS \cdot \eta_j = \sum_{j=1}^{6} \left[\omega_e^2 A_{ij} + i\omega_e B_{ij} \right]\eta_j,\ \ i = 1,\ 2,\ \ldots,\ 6 \tag{23}$$

where A_{ij} and B_{ij} are the added mass and damping coefficients matrices respectively, which can be written as

$$\begin{cases} A_{ij} = \dfrac{1}{\omega_e{}^2} \iint_{S_b} \left(u\dfrac{\partial\varphi_{Rj}}{\partial x} - \omega_e\varphi_{Ij} \right) n_i ds \\ B_{ij} = -\dfrac{1}{\omega_e} \iint_{S_b} \left(u\dfrac{\partial\varphi_{Ij}}{\partial x} + \omega_e\varphi_{Rj} \right) n_i ds \end{cases},\quad i, j = 1,2,\ldots,6 \tag{24}$$

where φ_{Rj} and φ_{Ij} is the real part and imaginary part of *j*-th potential. The wave excitation force can be obtained by the integration of incident and diffraction pressure as

$$F_i^{ext} = \iint_{S_b} (p_0 + p_7) n_i dS \cdot \eta_0 \tag{25}$$

The wave elevation on the free surface then can be obtained from the dynamic free surface boundary condition in the form

$$\zeta_j = \frac{i\omega_e}{g}\eta_j\varphi_j + \frac{1}{g}\nabla(\varphi_s - ux) \cdot \nabla(\eta_j\varphi_j) = \zeta_{Rj} + i\zeta_{Ij} \tag{26}$$

where ζ_{Rj} is the real part of *j-th* model, and ζ_{Ij} is the imaginary part.

3 Numerical implementation

In the numerical study, the boundary is divided into a number of quadrilateral panels with constant source density $\sigma_{(\xi)}$, where $\boldsymbol{\xi} = (\xi, \eta, \zeta)$ is the position vector on the boundary. If $\mathbf{x} = (x, y, z)$ is inside the fluid domain or on the boundary surface, the potential can be expressed by a source distribution on the boundary of the fluid domain:

$$\varphi(\vec{x}) = \iint_{S_b + S_f + S_c} \sigma(\vec{\xi}) G(\vec{x}, \vec{\xi}) dS_\xi \tag{27}$$

where φ denotes the steady potential φ_s or the unsteady potential φ_j, $G_{(x,\ \xi)}$ is the Rankine-type Green function that satisfies the sea bed boundary condition through the method of mirror image

$$\begin{aligned} G(\mathbf{x},\boldsymbol{\xi}) = &\frac{1}{\sqrt{(x-\xi)^2 + (y-\eta)^2 + (z-\varsigma)^2}} \\ &+ \frac{1}{\sqrt{(x-\xi)^2 + (y-\eta)^2 + (z+2d+\varsigma)^2}} \end{aligned} \tag{28}$$

If we have N panels on the body surface, free surface and control surface together, the potential in point **x** becomes

$$\varphi(\vec{x}_i) = \sum_{j=1}^{N} \frac{\sigma_j}{4\pi} \iint_{S_b + S_f + S_c} G(\vec{x}_i, \vec{\xi}) dS_\xi = \sum_{j=1}^{N} \frac{\sigma_j}{4\pi} G_{i,j} \tag{29}$$

When the collocation point and the panel are close to each other, the influence coefficients $G_{i,j}$ can be calculated with analytical formulas listed by Prins (1995) when the distance between the collocation point and the panel is large, these coefficients are calculated numerically. The same procedure can be applied to discretize the boundary integral for the velocity

$$\frac{\partial\varphi}{\partial n}(\vec{x}_i) = \frac{1}{2}\sigma_i + \sum_{\substack{j=1 \\ j\neq i}}^{N} \frac{\sigma_j}{4\pi} \iint_{S_b + S_f + S_c} \frac{\partial}{\partial n_i} G(\vec{x}_i, \vec{\xi}) dS_\xi = \frac{1}{2}\sigma_i + \sum_{\substack{j=1 \\ j\neq i}}^{N} \frac{\sigma_j}{4\pi} G^n_{i,j} \tag{30}$$

The analytical formulas of the influence coefficients $G^n_{i,j}$ are listed by Hess and Smith(1964).

The singularity distribution does not have to be located on the free surface itself, it can also be located at a short distance above the free surface, as long as the collocation points, where the boundary condition has to be satisfied, stay on the free surface. In practice, a distance of maximal three times the longitudinal size of a panel is possible (Bunnik, 1999). In the present study, the raised distance $\Delta z_i = \sqrt{S_i}$, where S_i is the area of the i-th panel.

Special attentions should be paid on the second derivative of the potential on the free surface. Generally, the difference schemes can be divided in two classes: up wind difference schemes and central difference schemes. Although central difference schemes are supposed to be more accurate, the stabilizing properties of the upwind difference schemes are more desired in the forward speed problem (Bunnik, 1999). Physically this can be explained by the face that new information on the wave pattern mainly comes from the upstream side, especially at high speeds, whereas the downstream side only contains old information. The second-order upwind difference scheme for the second derivative of the potential to x can be written as follows

$$\frac{\partial^2 \varphi}{\partial x^2}(\vec{x}_i) = \frac{1}{\Delta x^2}\left[\frac{1}{4}\varphi(\vec{x}_{i+4}) - 2\varphi(\vec{x}_{i+3}) + \frac{11}{2}\varphi(\vec{x}_{i+2}) - 6\varphi(\vec{x}_{i+1}) + \frac{9}{4}\varphi(\vec{x}_i)\right] \tag{31}$$

4 Results and discussions

The above theory is applied in our in-house developed 3D BEM program MHydro to investigate the side wall effects both in calm water and waves.

4.1 Side wall effects on experiments in calm water

4.1.1 Validations

Before we perform massive numerical calculations, a rigorous validation of the numerical program should be conducted. For wave-making problem, the validations are established on the open water tests of a Wigley III hull due the fact that there are considerable experiments data available. The model can be defined as

$$y = \frac{B}{2}\left[1 - \left(\frac{z}{D}\right)^s\right]\left[1 - \left(\frac{2x}{L}\right)^2\right]\left[1 + 0.2\left(\frac{2x}{L}\right)^2\right] \tag{32}$$

The main dimensions of Wigley III model is shown in Table 1. Fig. 2 shows the panel distribution on the computational domain.

Table 1 Main dimensions of Wigley III hull

Length, L (m)	3
Breadth, B (m)	0.3
Draught, D (m)	0.1875
Displacement, V (m^3)	0.078
Centre of rotation above base, KR (m)	0.1875
Centre of gravity above base, KG (m)	0.17
Radius of inertia for pitch, k_{yy} (m)	0.75

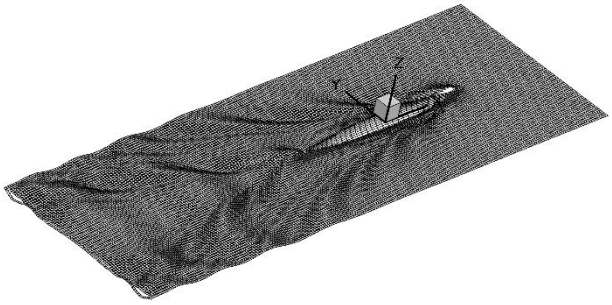

Fig. 2 The coordinate system and panel distribution on the computational domain of a Wigley III hull advancing in open calm water. There are 9,900 panels distributed on the half computational domain: 300 on the body surface of body surface and 9,600 on the free surface. The computational domain is truncated at *L* upstream and 2*L* downstream. The figure also shows the waves produced by Wigley hull at F_n = 0.3, where $F_n = u/\sqrt{gL}$ is the Froude number.

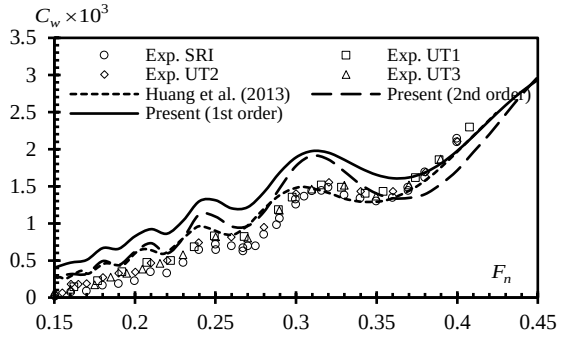

Fig. 3 Wave-making resistance coefficient of a Wigley hull. The experiments are conducted by Ship Research Institution (SRI), University of Tokyo (UT).

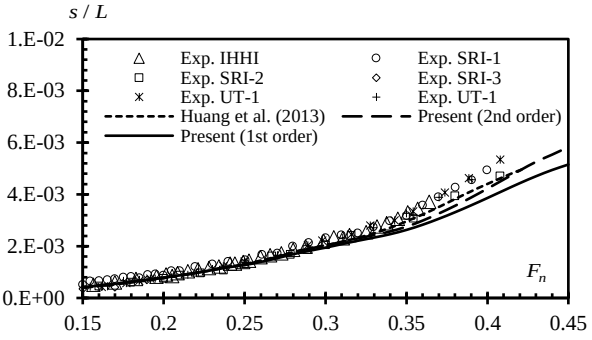

Fig. 4 Sinkage of a Wigley hull. IHHI indicates the experiments conducted by Ishikawajim-Harima Heavy Industries Co., Ltd..

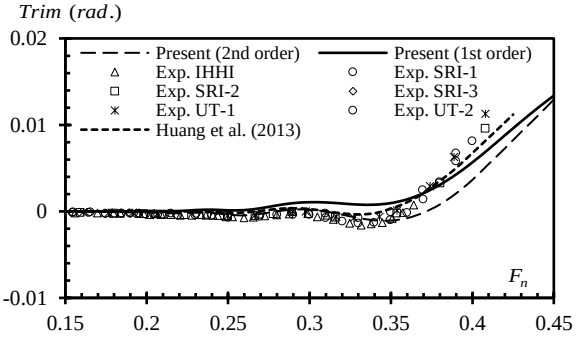

Fig. 5 Trim of a Wigley hull.

Fig. 3 shows the wave-making resistance results of a Wigley hull. The present results include both 1st order and 2nd order results. The 1st order results are obtained by solving the linear Newman-Kelvin free surface boundary condition in EQ. (6). The 2nd order results are obtained by solving 2nd order free surface boundary condition (Shahjada Tarafder and Suzuki, 2008). The numerical results from Huang et al. (2013) obtained from Neumann–Michell theory as well as the experimental measurements from different institutions are also included in the comparisons. Generally, the present program MHydro has a satisfactory predictions of the wave-making resistance. The 1st order method overestimates the wave-making resistance at $F_n < 0.35$, and at this range of Froude number, 2nd order results are more accurate. Regarding sinkage and trim (as shown in Fig. 4 and Fig. 5), the agreement between the present calculations and the experimental results are very well. The discrepancy becomes evident as the forward speed increases to $F_n > 0.35$. This is mainly due to the body surface boundary condition. As the speed of ship increases, the wave elevation increases significantly. At high speed case, the large wave elevation could modify the total wet surface of the ships. Therefore, the body surface boundary in EQ. (7) cannot only be satisfied on the mean wet surface. An instant wet body surface must be taken into consideration to account the nonlinear effects. The discussion about the nonlinearity of the body surface boundary condition can be found in Chen et al. (2016). In the present study, we aims to discuss the side wall effects and no attempt is made to discuss the nonlinearity of the body surface.

Fig. 6 shows the wave profiles along a Wigley hull with different forward speeds. The overall agreement between the present predictions and experimental results is very satisfactory. The discrepancies occur at the bow and stern parts, where the stagnation points are located. Besides, the 2nd order method provide a better prediction than 1st order linear method.

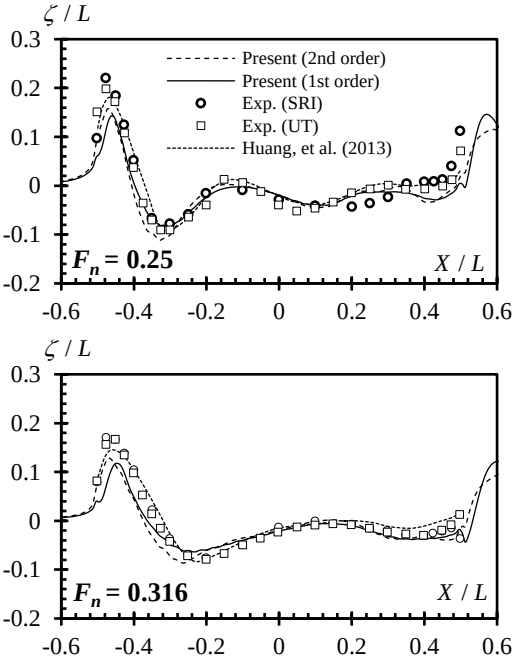

Fig. 6 Wave profiles along a Wigley hull with Froude number at F_n = 0.25 and F_n = 0.316.

4.1.1 Side wall effects

In order to simulate the side wall effect, we distribute source panels on the side walls, and the side wall boundary condition in EQ. (8) is applied. Fig. 7 presents the wave-making resistance coefficients at a wide range of d / L, where d is the transverse distance between the side wall and the center line of the ship. It can be concluded from Fig. 7 that at $F_n < 0.35$, the side wall effects can be neglected at $d / L > 0.3$. However, when conducting high speed test at $F_n > 0.35$, the breadth of the tank is required to be larger and the side wall effects can be neglected at $d / L > 0.4$. It can also be found the side wall effects are significant at $d / L = 0.2$. This is inconsistent with the theoretical estimation from EQ. (1), where the side wall effects are estimated to be vanished at $d / L > 0.18$. This is due to the near field local waves produced by the 3D ship, as shown in Fig. 8.

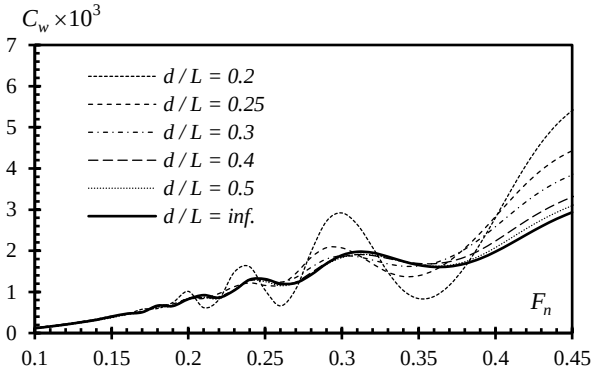

Fig. 7 Wave-making resistance coefficients at different d / L.

Fig. 8 (a) compares the wave elevation at $d / L = 0.5$ to the open water results with the same Froude number at $F_n = 0.3$. At the range of $X / L > -0.6$, the difference between open water results and the results with side walls can be hardly found. The Kelvin waves propagate to the far field downstream and strike the side wall at around $X / L = -1$, where a reflection occurs. The reflected waves modify the flow field at $X / L < -1$, while they can never strike the ship model. Therefore, the side wall effects can be neglected at $d / L = 0.5$. However, as shown in Fig. 8 (b), as the breadth of the tank becomes very small ($d / L = 0.2$), the wave field is completely modified by the reflected waves from the side walls. At $d / L = 0.2$, the waves produced by the bow propagate downstream and first trough strikes the side wall at around $X / L = 0.05$. The subsequent reflected waves (the trough) strike the stern of the ship, which reduces the pressure distribution on the stern. Therefore, the difference of the pressure on the bow and stern becomes evident and the wave-making resistance will suffer to an increase at $F_n = 0.3$, as shown in Fig. 7. However, it cannot be concluded that the wave-making resistance will increase as the breadth becomes smaller. It depends on the speed. As can be seen from Fig. 8 (c), at $F_n = 0.35$, the crest of the reflected wave strikes the stern, which enlarges the pressure distribution in the stern area. Therefore, the difference of the pressure on the bow and stern becomes smaller and the wave-making resistance at $F_n = 0.35$ is smaller than that in open water.

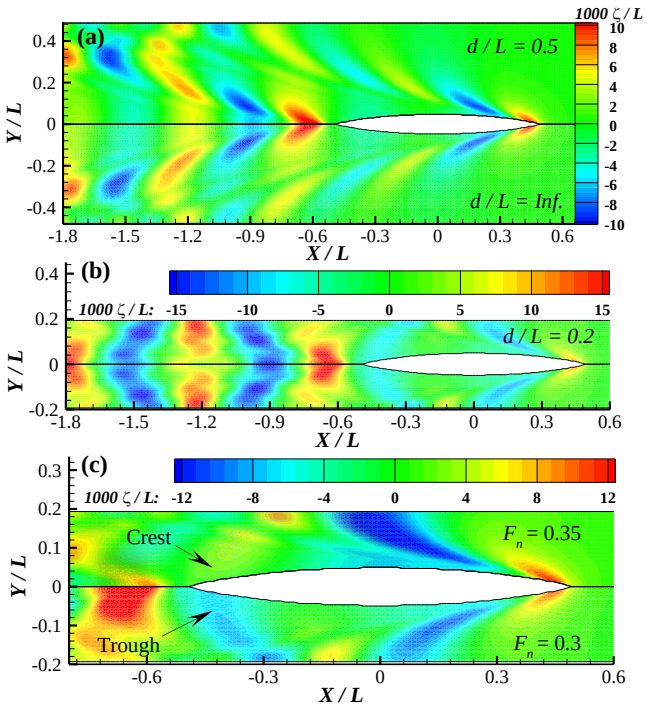

Fig. 8 Wave elevation on the free surface. (a) Upper half of the figure shows the wave elevation at d / L = 0.5 with Froude number at F_n = 0.3; lower half of the figure shows the wave elevation in open water with Froude number at F_n = 0.3; (b) wave elevation at d / L = 0.2 with Froude number at F_n = 0.3; (c) Upper half of the figure shows the wave elevation at d / L = 0.2 with Froude number at F_n = 0.35; lower half of the figure shows the wave at d / L = 0.2 with Froude number at F_n = 0.3.

4.2 Side wall effects on experiments in waves

4.1.1 Validations

The side wall effect on experiments in waves are more complicated than that in calm water. According to the asymptotic far field wave theory of a translating and oscillating singularity, there are at least three individual wave systems existing on the free surface, rather than a single Kelvin wave in calm water. It is well known that the far field patterns are determined by parameter τ (Noblesse and Hendrix, 1992; Yuan et al., 2015b). A critical value of τ is ¼, where the wave group travels the same speed with the singularity. In the previous studies, the difficulties arise from the proper radiation condition on the control surfaces at τ < ¼. We complemented a new radiation condition to the classical boundary value problem, which enables us to investigate the waves produced by a translating and oscillating object at τ < ¼ (Yuan et al., 2014a; Yuan et al., 2014b). In the present study, this radiation condition will be used to investigate the side wall effects on experiments in waves. Before we carry out massive numerical calculations, a rigorous validation of the numerical program should be conducted. Kashiwagi and Ohkusu's (1991) model test results will be used here to validate the numerical program.

The model used here is a half-immersed prolate spheroid of length L = 2.0 *m* and breadth B = 0.4 *m*. The model test was conducted in the towing tank (60 *m* length, 4 *m* breadth, 2.3 *m* in depth) of Nagasaki Institute of Applied Science. The model was advancing at a Froude number F_n = 0.1 in the waterway of d / L = 1.0. In the numerical calculation, 6324 panels are distributed on the half domain of the symmetrical boundaries (404 panels on the body surface, 4,800 on the free surface, 640 on the side walls and 480 on the control surfaces), as shown in Fig. 9. The free surface is truncated at L upstream and 2L downstream.

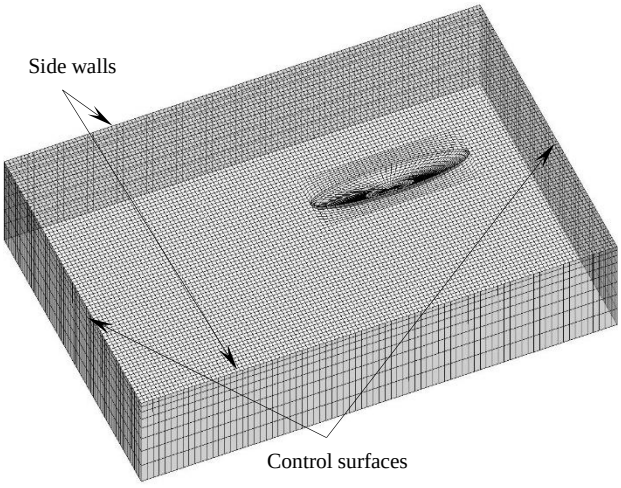

Fig. 9 Panel distribution on a half-immersed prolate spheroid advancing in a towing tank of d / L = 1.0.

Fig. 10 and Fig. 11 show the hydrodynamic coefficients. In general, the present calculations from MHydro agree well with the experimental measurements as well as the numerical results based on slender ship theory. As the parameter $\tau < 0.25$, the hydrodynamic coefficients (radiation forces) fluctuate violently away from the open sea results. The existence of the side wall can be treated by the mirror image method, which has been widely used to deal with the sea bottom boundary condition. Thus, as $\tau < 0.25$, the radiated waves from the mirrored spheroid can propagate to the domain where the spheroid is located and strike the spheroid. It can also be observed the agreement between the present calculations and experiments is very satisfactory even at parameter $\tau < 0.25$, which indicates the radiation condition included in the present numerical program MHydro is capable to predict the hydrodynamic properties of the advancing ships even at parameter $\tau < 0.25$. As the parameter τ increases, the hydrodynamic coefficients gradually approach the open sea results and the side wall effects trend to diminish. Fig. 12 shows the wave exciting forces of a half-immersed prolate spheroid of B / L = 1/5 in waterway of d / L = 1.0 (F_n = 0.1). Both of the heave force and pitch moment agree well with the experimental measurements as well as the published numerical results based on slender ship theory (Kashiwagi and Ohkusu, 1991). A very large spike can be observed at λ / L = 1.47, which corresponds to τ = 0.25. This is due to the fact that the reflected waves from the side wall could strike the spheroid. It can be found from Yuan et al. (2015c) that as the parameter τ increases, the semi-wedge angle becomes smaller. Therefore, the reflecting point shifts downstream and less of the reflected waves can strike the ship model. The steady wave system is a special case of parameter $\tau = 0$, when speed is nonzero while the oscillating frequency is zero. In this case, the unsteady problem in waves reduces to steady

problem in calm water.

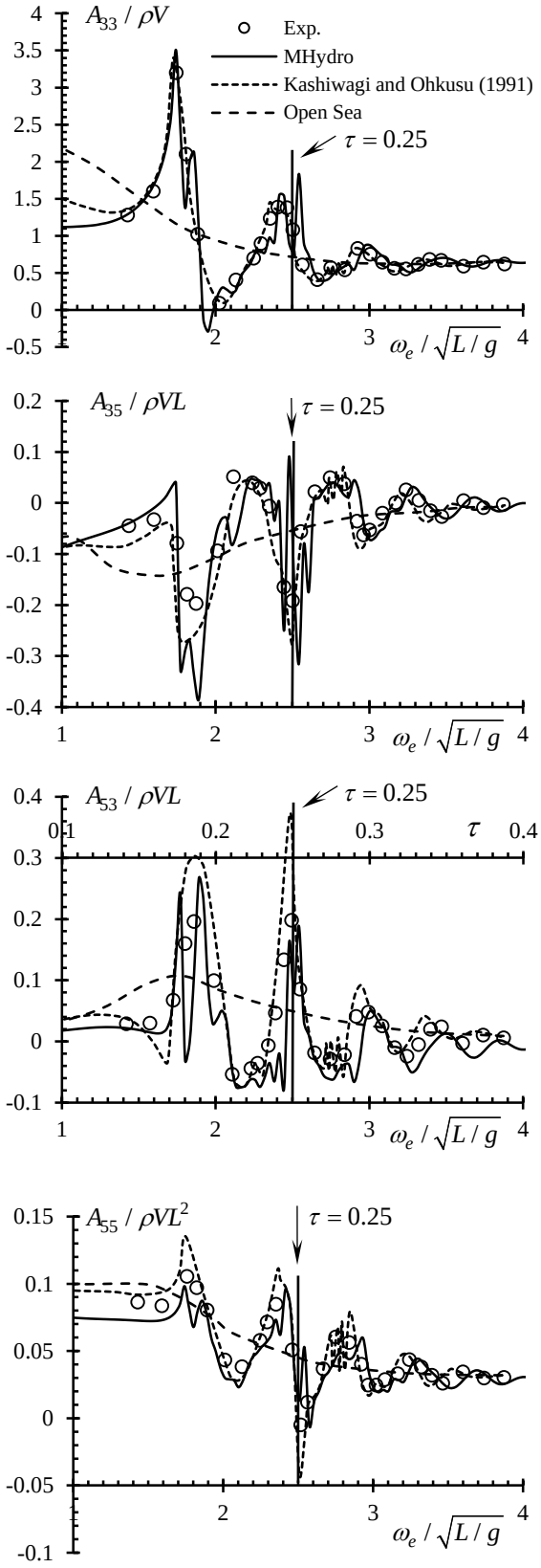

Fig. 10 Added mass of a half-immersed prolate spheroid of B / L = 1/5 in waterway of d / L = 1.0 (F_n = 0.1).

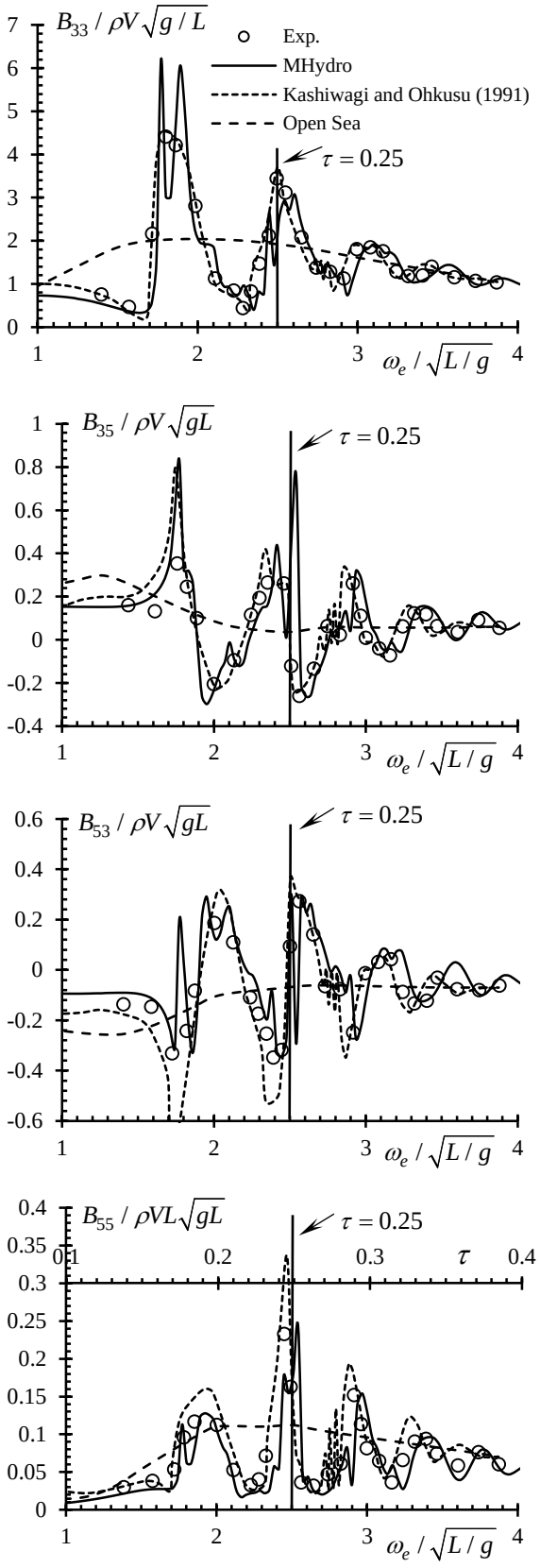

Fig. 11 Damping of a half-immersed prolate spheroid of B / L = 1/5 in waterway of d / L = 1.0 (F_n = 0.1).

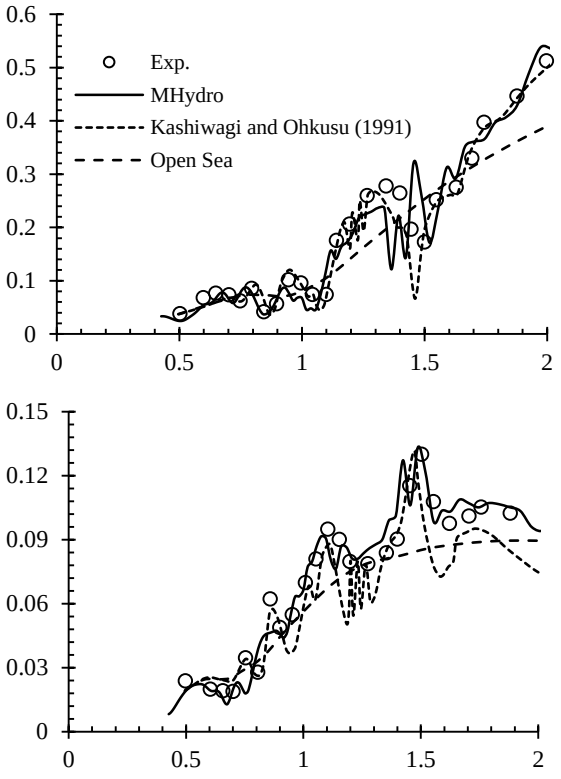

Fig. 12 Wave exciting forces of a half-immersed prolate spheroid of B / L = 1/5 in waterway of d / L = 1.0 (F_n = 0.1).

As described above, a jump of side wall effects was observed at parameter τ = 0.25. We plot the wave elevation at τ = 0.25 and a very interesting phenomenon occurs: the reflected waves are trapped in the towing tank and they are not propagating downstream (as shown in Fig. 13). These reflected wave of course will strike the ship model which affects the hydrodynamics of the model significantly. We also present the wave elevation at τ = 0.5 in Fig. 14. There are different patterns of reflected waves downstream of the model. But these waves are not trapped and they cannot strike the ship model. Therefore, as the parameter becomes very large, the side wall effects diminish in the towing tank.

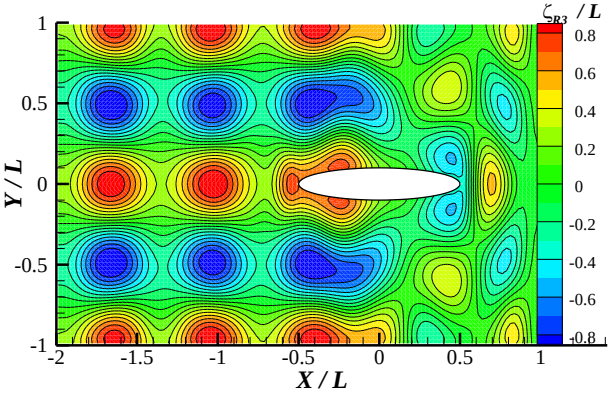

Fig. 13 Real part of radiated waves for unit heave motion of a half-immersed prolate spheroid of B / L = 1/5 in waterway of d / L = 1.0 (F_n = 0.1, τ = 0.25).

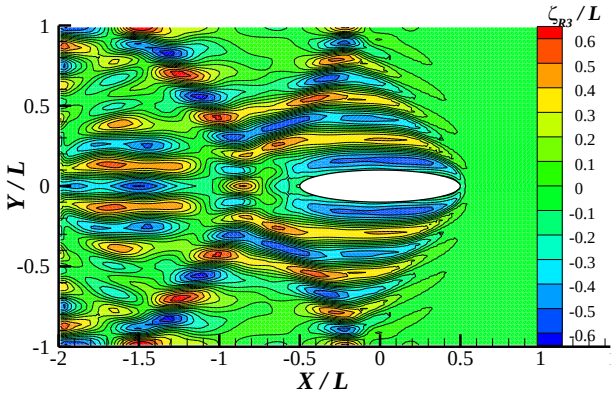

Fig. 14 Real part of radiated waves for unit heave motion of a half-immersed prolate spheroid of B / L = 1/5 in waterway of d / L = 1.0 (F_n = 0.1, τ = 0.25).

4.2 Diagram of side wall effects

As can be seen from Fig. 10 to Fig. 12, the side wall effects diminish gradually as the nondimensional frequency increases to a certain value. During the calculation, we find for any given Froude number, we can always find a critical frequency showing the existence of the side wall effects. Therefore, we can determine the critical lines showing the existence of the side wall effects as a function of Froude number, frequency and transverse distance. Results are shown in Fig. 15, where x-axis is the $\sqrt{g/L}/\omega_e = F_n/\tau$, y-axis is F_n. The ratio of y to x is parameter τ. In the present numerical calculation, for a given value of d / L, the critical parameter τ is unique. Therefore, the dashed lines in Fig. 15 are linear and they represent the critical line estimated from the asymptotic far-field wave theory (Yuan et al., 2015c). The solid curves are the calculated critical lines, which approach the dotted lines at high frequency, where the wavelength is relatively small compared to the transverse distance and the theoretical estimation is valid. As the encounter frequency decreases, the discrepancies become evident and the range of side wall effects expands. The difference between the dashed lines and solid curves is due to the effect of the near-field non-radiation local waves in the vicinity of the ship model.

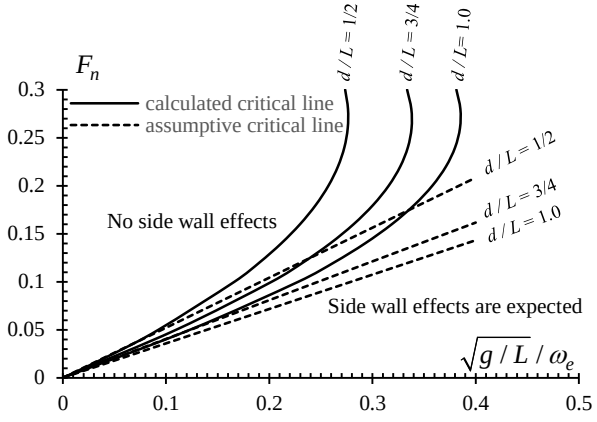

Fig. 15 Theoretical and numerical estimation of the critical lines showing whether the side wall effects are expected.

5 Conclusions

In this paper, a boundary element program based on 3-D Rankine source method was developed to predict the side wall effects during ship model tests in the towing tank. We investigated the side wall effects on ship model tests both in calm water and waves. It was found in calm water case, the side wall effects can be neglected at $d / L > 0.4$. A significant side wall effects were observed at $d / L = 0.4$ due to the reflected waves from the side walls. The side wall effects in calm water are main determined by two factors: the transverse distance (d) between the ship and side wall and the speed (u) of the ship model. The side wall effects for a combination of d and u are uncertain. It depends on the reflected waves. When the crest strikes the model, the resistance becomes smaller than that in open water, while the model is stroke by the trough, the wave-making resistance increases. The side wall effect on experiments in waves are more complicated than that in calm water due to the complexity of the wave systems. Compared to the calm water case, there is one more critical factor which determines the side wall effects in waves. That is parameter τ. As the parameter $\tau < 0.25$, the hydrodynamic coefficients (radiation forces) fluctuate violently away from the open sea results. As the parameter τ increases, the hydrodynamic coefficients gradually approach the open sea results and the side wall effects trend to diminish. At parameter $\tau = 0.25$, a very interesting phenomenon was observed: the reflected and radiated waves are trapped within the towing tank and the side wall effects becomes significant.

We also depicted a diagram showing whether the side wall effects are expected based on a massive numerical calculations. From the diagram, an evident discrepancy was observed between the theoretical estimation and numerical calculation, especially at the low frequency range. The theoretical estimation based on asymptotic far-field wave pattern under-estimated the range of the side wall effects. In practice, due to the near-field local waves, the side wall exists in a wider range.

Acknowledgement

The work reported in this paper was performed within the project “Energy Efficient Safe Ship Operation (SHOPERA)” funded by the European commission under contract No. 605221.

References

Beck, R.F., Newman, J.N., Tuck, E.O., 1975. Hydrodynamic forces on ships in dredged channels. *Journal of Ship Research* 19 (3), 166–171.

Becker, E., 1958. Das Wellenbild einer unter der Oberfläche eines Stromes schwerer Flüssigkeit pulsierenden Quelle. *Journal of Applied Mathematics and Mechanics* 38 (9-10), 391-399.

Bunnik, T., 1999. Seakeeping calculations for ships, taking into account the non-linear steady waves, PhD thesis. Delft University of Technology, The Netherlands.

Chen, X., Zhu, R., Ma, C., Fan, J., 2016. Computations of linear and nonlinear ship waves by higher-order boundary element method. *Ocean Engineering* 114, 142-153.

Hess, J.L., Smith, A.M.O., 1964. Calculation of nonlifting potential flow about arbitrary three-dimensional bodies. *Journal of Ship Research* 8 (2), 22-44.

Hosoda, R., 1976. Side wall effects of towing tank on the results of experiments in wave. J*ournal of the Society of Naval Architects of Japan* 143, 52-60.

Huang, F., Yang, C., Noblesse, F., 2013. Numerical implementation and validation of the Neumann–Michell theory of ship waves. *European Journal of Mechanics - B/Fluids* 42, 47-68.

Iwashita, H., 2001. Side wall effect of towing tank on measured unsteady waves in low frequency range, *16th International Workshop on Water Waves and Floating Bodies*, Hiroshima, Japan.

Kashiwagi, M., Ohkusu, M., 1989. Side-Wall Effects on Hydrodynamic Forces Acting on a Ship with Forward and Oscillatory Motions, *5th International Conference on Numerical Ship Hydrodynamics*, Hiroshima, Japan.

Kashiwagi, M., Ohkusu, M., 1991. A new theory for side-wall interference effects on forward-speed radiation and diffraction forces. *Ship Technology Research* 38 (1), 17-48.

Mei, C.C., Choi, H.S., 1987. Forces on a slender ship advancing near the critical speed in a wide canal. *Journal of Fluid Mechanics* 179, 59-76.

Newman, J.N., 1976. Linearized wave resistance, *International Seminar on Wave resistance*, Tokyo.

Newman, J.N., 1978. The theory of ship motion. *Advances in Applied Mechanics* 18 (221-283).

Noblesse, F., Hendrix, D., 1992. On the theory of potential flow about a ship advancing in waves. *Journal of Ship Research* 36 (1), 17-30.

Norrbin, N.H., 1974. Bank effects on a ship moving through a short dredged channel, *Symposium on Naval Hydrodynamics (10th), Cambridge*, Mass, June 24-28, 1974.

Prins, H.J., 1995. Time domain calculations of drift forces and moments, PhD Thesis. Delft University of Technology, The Netherlands.

Shahjada Tarafder, M., Suzuki, K., 2008. Numerical calculation of free-surface potential flow around a ship using the modified Rankine source panel method. *Ocean Engineering* 35 (5-6), 536-544.

Takaki, M., 1979. Effects of breadth and depth of restricted waters on longitudinal motions in waves. *Journal of the Society of Naval Architects of Japan* 146, 173-184

Tuck, E.O., 1978. Hydrodynamic Problems of Ships in Restricted Waters. *Annual Review of Fluid Mechanics* 10 (1), 33-46.

Yuan, Z.-M., Incecik, A., Dai, S., Alexander, D., Ji, C.-Y., Zhang, X., 2015a. Hydrodynamic interactions between two ships travelling or stationary in shallow waters. *Ocean Engineering* 108, 620-635.

Yuan, Z.-M., Incecik, A., Day, A., Jia, L., 2015b. Double Doppler shift theory on water waves generated by a translating and oscillating source, *30th Intl Workshop on Water Waves and Floating Bodies*, Bristol, UK.

Yuan, Z.-M., Incecik, A., Day, A.H., 2014a. Verification of a new radiation condition for two ships advancing in waves. *Applied Ocean Research* 48, 186-201.

Yuan, Z.-M., Incecik, A., Ji, C.-Y., Zhao, W., Day, A., 2015c. Theoretical and numerical estimation of ship-to-ship hydrodynamic interaction effects. Submitted to *Ocean Engineering*.

Yuan, Z.-M., Incecik, A., Jia, L., 2014b. A new radiation condition

for ships travelling with very low forward speed. *Ocean Engineering* 88, 298-309.

Yuan, Z.M., He, S., Paula, K., Incecik, A., Turan, O., Boulougouris, E., 2015d. Ship-to-Ship Interaction during Overtaking Operation in Shallow Water. *Journal of Ship Research* 59 (3), 172-187.